Gust Acoustics Computation with a Space-Time CE/SE Parallel 3D Solver

X.Y. Wang[1] and A. Himansu[2] and S.C. Chang[3] and P.C.E. Jorgenson[4]

[1,2]Taitech Inc., NASA Glenn Research Center, Cleveland, Ohio
[3,4]NASA Glenn Research Center, Cleveland, Ohio
email: [1]*wangxy@turbot.grc.nasa.gov*, [2]*fshiman@suspiria.grc.nasa.gov*
email: [3]*sin-chung.chang@grc.nasa.gov*, [4]*jorgenson@grc.nasa.gov*

Key Words: GUST ACOUSTICS, SPACE-TIME CE/SE 3D SOLVER

Abstract. The benchmark Problem 2 in Category 3 of the Third Computational Aero-Acoustics (CAA) Workshop is solved using the space-time conservation element and solution element (CE/SE) method. This problem concerns the unsteady response of an isolated finite-span swept flat-plate airfoil bounded by two parallel walls to an incident gust. The acoustic field generated by the interaction of the gust with the flat-plate airfoil is computed by solving the 3D Euler equations in the time domain using a parallel version of a 3D CE/SE solver. The effect of the gust orientation on the far-field directivity is studied. Numerical solutions are presented and compared with analytical solutions, showing a reasonable agreement.

1 Introduction

The noise generated by the interaction of vortical disturbances originating upstream with propeller or turbomachinery blades has been of great interest in noise studies. A model problem regarding a one-dimensional vortical wave interaction with an isolated finite-span swept flat-plate airfoil bounded by two parallel walls was posed as a benchmark problem in Category 3 of the Third CAA Workshop [1]. The effect of different gust orientations on the far-field directivity is investigated here.

This problem is solved numerically by solving the unsteady 3D Euler equations in the time domain using the space-time conservation element and solution element (CE/SE) method. The CE/SE method is an innovative numerical method [2–5]. It applies flux conservation to finite space-time volumes, and achieves second-order accuracy in both space and time for uniform space-time meshes. Its salient properties are summarized briefly as follows. First, both local and global flux conservations are enforced in space and time instead of in space only. Second, all the dependent variables and their spatial derivatives are considered as individual unknowns to be solved for simultaneously at each grid point. Third, every CE/SE scheme is based upon a non-dissipative scheme with addition of fully controllable numerical dissipation. This results in very low numerical dissipation. Fourth, the flux-based specification of the CE/SE schemes gives rise in a natural fashion to a simple

yet generally effective non-reflecting boundary condition, which is an important issue in CAA. A detailed description of this method and accompanying analysis can be found in [2–7]. Applications of this method to CAA problems reveal that the CE/SE method can produce accurate results in a simple way [8–11].

In this paper, a parallel version of the 3D CE/SE Euler solver is used to compute the acoustic field generated by the interaction of a vortical gust with an isolated swept flat-plate airfoil bounded by two parallel walls. Different spanwise wavenumbers of the gust are used to investigate the far-field directivity.

In the following, the description of the benchmark problem is given first, which is followed by the boundary and initial conditions used in the calculation, and numerical results and discussion.

2 Gust - Flat-Plate Airfoil Problem

Consider an isolated finite-span swept flat-plate airfoil bounded by two parallel walls shown in Fig. 1. The x-axis is aligned with the chord of the airfoil, the y-axis is perpendicular to it and the z-axis is normal to the bounding walls. The normal distance between walls, h, is $2.6c$, where c is the chord length of the flat plate. The sweep angle of the flat-plate airfoil is 15°.

The mean flow is assumed to be uniform and aligned with the x-axis. The mean flow variables are inflow velocity, U_0, static density, ρ_0, and static pressure, p_0. The inflow Mach number, M_0, is 0.5. Flow variables are nondimensionalized by using a_0(the speed of sound) as the velocity scale, c as the length scale, c/a_0 as the time scale, ρ_0 as the density scale and $\rho_0 a_0^2$ as the pressure scale. Thus the mean flow is described in dimensionless variables as

$$\bar{\rho} = 1, \quad \bar{u} = 0.5, \quad \bar{v} = 0, \quad \bar{w} = 0, \quad \bar{p} = 1/\gamma \tag{1}$$

where γ is the specific heat ratio and assumed to be 1.4.

The incident gust carried by the mean flow has x, y, and z velocity components given by

$$u' = 0, \quad v' = v_G \cos(k_x x + k_z z - \omega t), \quad w' = 0 \tag{2}$$

respectively, where $v_G = 0.05$ and $k_x = 5.5, k_z = 3.6m$, with $m = 0, 1, 2$, and $\omega = M_0 k_x$, respectively. The corresponding period of the gust wave is $T = 2\pi/\omega$. It is assumed that the gust is "frozen" and convected by the uniform mean flow. Thus the gust satisfies the linearized Euler equations. This implies that $\rho' = p' = 0$.

The gust is convected by the mean flow and interacts with the swept flat-plate airfoil. Thus, acoustic waves are generated which propagate both upstream and downstream. Let $(u^*, v^*, w^*, p^*, \rho^*)$ represent the unsteady solution due to the propagating acoustic waves, and define

$$\hat{u} = \bar{u} + u^*, \quad \hat{v} = \bar{v} + v^*, \quad \hat{w} = \bar{w} + w^*, \quad \hat{p} = \bar{p} + p^*, \quad \hat{\rho} = \bar{\rho} + \rho^*, \quad (3)$$

which represent the mean flow and the acoustic waves. Thus, we have

$$u = \hat{u} + u', \quad v = \hat{v} + v', \quad w = \hat{w} + w', \quad p = \hat{p} + p', \quad \rho = \hat{\rho} + \rho', \quad (4)$$

where (u, v, w, p, ρ) is the solution of the total flowfield, including the mean flow, the gust, and the acoustic waves.

In the current computation, the mean flow and the acoustic waves $(\hat{u}, \hat{v}, \hat{w}, \hat{p}, \hat{\rho})$ are computed by solving the nonlinear Euler equations. The convection of the gust is not simulated here.

3 Initial and Boundary Conditions

At $t = 0$, the time-marching variables in the whole domain are defined using the mean flow variables, and their spatial derivatives are set as zero. At the inlet, outlet, and the open boundary in y- direction, the time-marching variables and their spatial derivatives at the nth time level, are specified using the $(n - 1/2)$th time level value of the corresponding variables at the interior spatial point of its immediate neighbor. It allows the flux to "stream" out of the spatial domain smoothly with minimal reflection [7].

On the top and bottom walls bounding the flat-plate airfoil and the flat-plate airfoil surface, it is assumed that the velocity (u, v, w) is tangent to the wall/airfoil surface. By using Eq. (4), this implies that

$$n_x\hat{u} + n_y\hat{v} + n_z\hat{w} = -(n_x u' + n_y v' + n_z w') \quad (5)$$

where (n_x, n_y, n_z) is any unit vector normal to the wall/airfoil surface at the point under consideration.

On the symmetric plane at $y = 0$, the anti-symmetric condition is used for the solution of the acoustic waves as follows:

$$p^*(x, -y, z) = -p^*(x, y, z), \quad \rho^*(x, -y, z) = -\rho^*(x, y, z), \quad u^*(x, -y, z) = -u^*(x, y, z), \quad v^*(x, -y, z) = v^*(x, y, z), \quad w^*(x, -y, z) = -w^*(x, y, z) \quad (6)$$

No grid points are located at the flat-plate airfoil leading and trailing edges, in order to avoid the singular flow behavior.

4 Numerical Results and Discussion

A structured 281x71x41 hexahedral grid is generated by using an algebraic transformation in the computational domain of $-7 \leq x \leq 7$, $0 \leq y \leq 7$, and $0 \leq z \leq h$ first. A slice of the grid in x-z planes is shown in Fig. 2. Each hexahedron is cut into six tetrahedrons, which results in 4704000(280x70x40x6) tetrahedral cells in the computation. The parallel version of the 3D Euler

solver is used with $\alpha = 0$ and $\epsilon = 0.5$, where α and ϵ are the parameters connected with the specification of the numerical dissipation in the solver [5]. A detailed description of the 3D Euler solver is referred to in [5] and the parallelization part is given in [6]. In the current computation, $\Delta t = T/168$ is used.

The spanwise wavenumber $k_z = 3.6m$ with $m = 0, 1, 2$, corresponding to three different gust orientations, are used here to study its effect on the far-field directivity. The analytical solution of the RMS acoustic pressure on the circle of radius 5 centered at $(0, 0, h/2)$ on the middle plane between the two bounding walls is available to compare with the corresponding numerical result. In all figures, the acoustic pressure p^* non-dimensionalized by v_G is plotted. The time history of the acoustic pressure at point $(-5, 0, h/2)$, which is located at the upstream on the specified circle, is shown in Fig. 3 for the three different values of m. It can be seen that (i) the solution is fully converged by $t = 50T$ for $m = 0$; (ii) a slight variation in the maximum absolute value of the acoustic pressure is still observed for $m = 1$ and 2; and (iii) the absolute amplitude of the acoustic pressure at the upstream decreases when the value of m increases. The solution convergence is also checked by comparing the RMS acoustic pressure on the specified circle at $t = 40T$ and $t = 50T$, which shows to be identical.

The computed result of the RMS acoustic pressure on the specified circle normalized by the maximum RMS pressure value at $m = 0$ is plotted in Fig. 4, while the corresponding analytical solution taken from [1] is reproduced in Fig. 5. It can be seen that both computed and analytical solutions show that the RMS pressure decreases when the spanwise wavenumber increases. The computed far-field radiation pattern is similar to those shown in the analytical solution. However some discrepancies are also observed, which is possibly caused by the non-reflecting boundary conditions used in the computation. Some reflections are created at the outer boundaries. A larger computational domain can be used to reduce the reflection errors from the outer boundary. However, a larger domain involves extensive mesh points and the computational cost is too expensive.

The parallel 3D CE/SE code was run on Origin2000 clusters. For a mesh of 4704000 cells, it takes around 35 hrs of wall-clock time to reach $t = 50T$ (16800 time iterations) using 32 CPUs.

5 Conclusion

The Problem 2 in Category 3 of the Third CAA Workshop has been solved by using the 3D parallel CE/SE Euler solver. The numerical results of the acoustic RMS pressure on the circle of radius 5 centered at $(0, 0, h/2)$ on the middle plane between two bounding walls are compared with the analytical solution for three different gust orientations, showing a reasonable agreement.

6 Acknowledgment

This work was supported by NASA Glenn Research Center through Contract NAS3-97186. The first author would like to thank Dr. Edmane Envia for his valuable help in this work.

References

[1] The Proceeding of the Third Computational Aeroacoustics (CAA) Workshop on Benchmark Problems, NASA/CP-2000-209790, August, 2000.

[2] S.C. Chang, "The Method of Space-Time Conservation Element and Solution Element – A New Approach for Solving the Navier-Stokes and Euler Equations," *J. Comput. Phys.*, **119,** pp. 295-324, (1995).

[3] S.C. Chang, X.Y. Wang, and C.Y. Chow, "The Space-Time Conservation Element and Solution Element Method – A New High-Resolution and Genuinely Multidimensional Paradigm for Solving Conservation Laws," *J. Comput. Phys.*, **156**, pp. 89–136, (1999).

[4] X.Y. Wang and S.C. Chang, "A 2D Non-splitting Unstructured-triangular-mesh Euler Solver based on the Method of Space-Time Conservation Element and Solution Element," Vol. 8, No. 2, pp. 326-340, 1999, *Computational Fluid Dynamics JOURNAL.*

[5] X.Y. Wang and S.C. Chang, "A 3D Non-splitting Structured/Unstructured Euler Solver based on the Method of Space-Time Conservation Element and Solution Element," AIAA Paper 98-3278, Norfolk, Virginia, June, 1998.

[6] A. Himansu, P. Jorgenson, X.Y. Wang and S.C. Chang, "Parallel CE/SE Computations via Domain Decomposition," in *Proceedings of 1st International Conference of Computational Fluid Dynamics*, Kyoto, June, 2000.

[7] S.C. Chang, A. Himansu, C.Y. Loh, X.Y. Wang, S.T. Yu and P.C.E. Jorgenson, "Robust and Simple Non-Reflecting Boundary Conditions for the Space-Time Conservation Element and Solution Element Method," AIAA Paper 97-2077, June 29-July 2, 1997, Snowmass, CO.

[8] C.Y. Loh, L.S. Hultgren and S.C. Chang, "Waves Computations in Compressible Flow Using the Space-Time Conservation Element and Solution Element method," *AIAA Journal*, Vol.39, No.5, pp. 794–801, May 2001.

[9] X.Y. Wang, C.Y. Chow and S.C. Chang, "Numerical Simulation of Gust Generated Aeroacoustics in a Cascade Using the Space-Time Conservation Element and Solution Element Method," AIAA Paper 98-0178, January 12-15, 1998, Reno, NV.

[10] X.Y. Wang, A. Himansu, P. Jorgenson, and S.C. Chang, "Gust Acoustic Response of a Swept Rectilinear Cascade Using the Space-Time CE/SE Method," FEDSM 2001-18134, in *Proceedings of FEDSM'01 2001 Fluids Engineering Summer Meeting*, May 29–June 1, 2001.

[11] X.Y. Wang, S.C. Chang, A. Himansu, and P. Jorgenson, "Gust Acoustic Response of a Single Airfoil Using the Space-Time CE/SE Method," AIAA 2002-0801, Reno, NV, January, 2002.

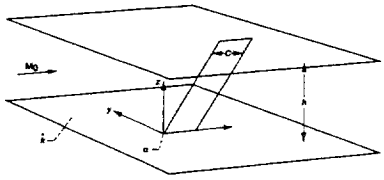

Fig. 1. Geometry of an isolated finite-span, swept flat-plate airfoil bounded by two walls.

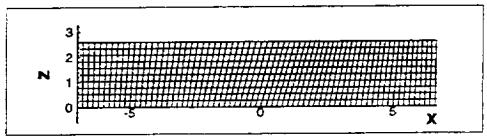

Fig. 2. A slice of the hexahedral mesh in the x-z plane.

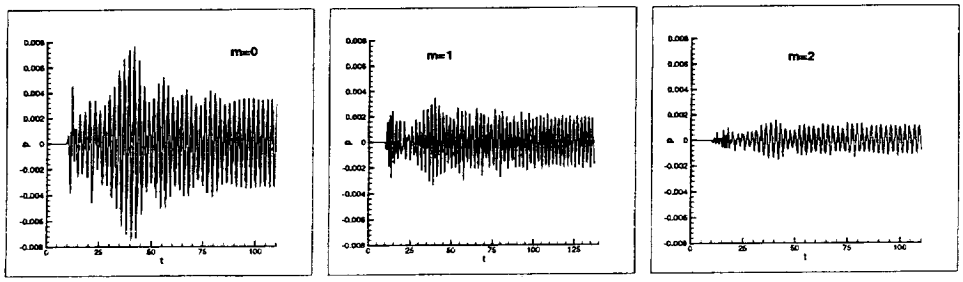

Fig. 3. The time history of the acoustic pressure at point $(-5, 0, h/2)$ for the three different values of m..

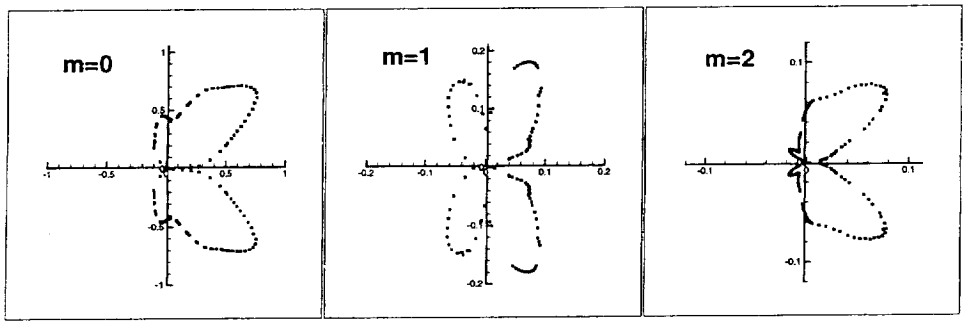

Fig. 4. The computed directivity pattern (RMS pressure on a circle of radius 5 centered at point $(0, 0, h/2)$ on the plane of $z = h/2$) for the three different values of m.

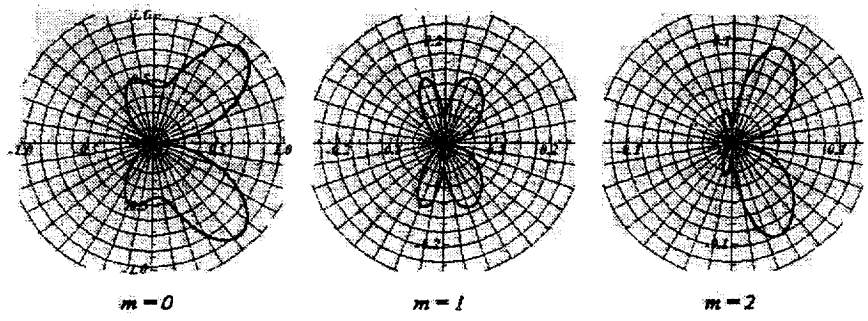

Fig. 5. The corresponding directivity pattern exhibited by the analytical solution for the three different values of m.